JOURNAL OF MATERIALS SCIENCE **37** (2002) 197–202

Effect of cerium zirconate ($Ce_2Zr_2O_7$) on microstructure and mechanical properties of Ce-ZTA

V. V. MISHRA, A. SAHA*, D. C. AGRAWAL‡
Materials Science Programme, I.I.T. Kanpur, Kanpur-208016, India

Powders for ZrO_2 toughened Al_2O_3 (ZTA) composites containing 8, 11, 13.8 and 16.5 vol% ZrO_2 (stabilized with 11.5 mol% CeO_2) are prepared by a hybrid sol-gel method using Al_2O_3 powders and a sol formed from Zr-alkoxide and cerium nitrate. Besides ZrO_2, a small amount of a Ce-zirconate phase ($Ce_2Zr_2O_7$) forms when the powders are calcined in air. The zirconate phase persists in the sintered specimens and its amount increases from surface to centre of the specimen. Presence of higher amount of $Ce_2Zr_2O_7$ promotes exaggerated grain growth of Al_2O_3. Particles of Zr rich phases are found to be trapped inside the Al_2O_3 grains. Composites exhibit higher fracture toughness despite lower transformability of t-ZrO_2 during fracture when they contain high amount of zirconate. Crack bridging is shown to be an important mechanism contributing to enhancement in fracture toughness in these composites.

1. Introduction

ZrO_2 toughened Al_2O_3 (ZTA) finds wide application owing to its high fracture toughness and strength. The stress induced tetragonal to monoclinic (t → m) transformation usually provides the major contribution to enhanced mechanical properties in ZrO_2 toughened ceramics. The metastable tetragonal phase of ZrO_2 added to ceramic is obtained by addition of oxides like Y_2O_3, CeO_2 etc. In CeO_2 stabilized tetragonal zirconia polycrystal (TZP), a Ce-zirconate phase ($Ce_2Zr_2O_7$) having a pyrochlore structure separates out when the ceramic is subjected to high temperature (>1000°C) annealing in vacuum or in a reducing atmosphere [1]. The formation of $Ce_2Zr_2O_7$ is due to the reduction of Ce^{4+} to Ce^{3+}. The reduced availability of CeO_2 causes the tetragonal phase to be partially or fully destabilized, transforming it to the monoclinic phase [2, 3]. Heussner *et al*. [2] demonstrated that the increased t → m transformation, due to the formation of $Ce_2Zr_2O_7$ generates compressive stresses on the surface of the 12 mol% Ce-TZP and enhances its strength from 245 to 545 MPa. Xue *et al*. [4] found that the presence of Ce^{3+} in ZTA enhances the grain boundary mobility of Al_2O_3; the ZrO_2 particles, above a certain size, break-away from Al_2O_3 grain boundaries. This produces a microstructure consisting of intragranular ZrO_2 located in large Al_2O_3 grains. Although significant change in microstructure of ZTA due to reduction of Ce^{4+} to Ce^{3+} is reported, however, the effect of $Ce_2Zr_2O_7$ on the microstructure and mechanical properties of ZTA has not been studied. In the present investigation, the effect of $Ce_2Zr_2O_7$ on the mechanical properties of ZTA has been studied. Crack bridging mechanism is shown to be operative in ZTA containing high amounts of zirconate and leads to enhancement in toughness despite lower transformability of t-ZrO_2.

2. Experimental

Al_2O_3-ZrO_2 composites containing 8, 11, 13.8 and 16.5 vol% ZrO_2 (stabilized with 11.5 mol% CeO_2) are fabricated by hybrid sol-gel technique [5]. A sol based on Zr-n-propoxide (Zr-n-p) with composition Zr-n-p: acetic acid:isopropanol :: 1 : 1 : 20 (molar) is prepared. First Zr-n-p is added to acetic acid and is stirred for 10 minutes. Half of the propanol is then added to it and stirring is continued for 30 minutes. A solution of $Ce(NO_3)_3{\cdot}6H_2O$ is prepared separately by dissolving the required amount of the nitrate salt to the rest of the propanol. Then the nitrate solution is added drop by drop to the sol and stirred for another 30 minutes. The pH of the sol is found to be ∼5. Al_2O_3 powder is added to the sol with continuous stirring and the resulting slurry is ultrasonicated to ensure complete break up of the Al_2O_3 agglomerates. Triple distilled water in the ratio of Zr-n-p:water :: 1 : 4 (molar) is added to the slurry leading to gelation. The gel is oven dried at 100°C for 24 hours and subsequently crushed lightly in a mortar pestle and sieved through 70–80 mesh. The calcination of powders is carried out at 600°C for 2 h in air. The calcined powders are mixed with PVA solution as binder so as to yield 1 wt% PVA in the powder. The powders are uniaxially pressed into circular pellets of

Present Address: Department of Mechanical Engineering, University of Colorado, Boulder, USA.
‡Author to whom all correspondence should be addressed.

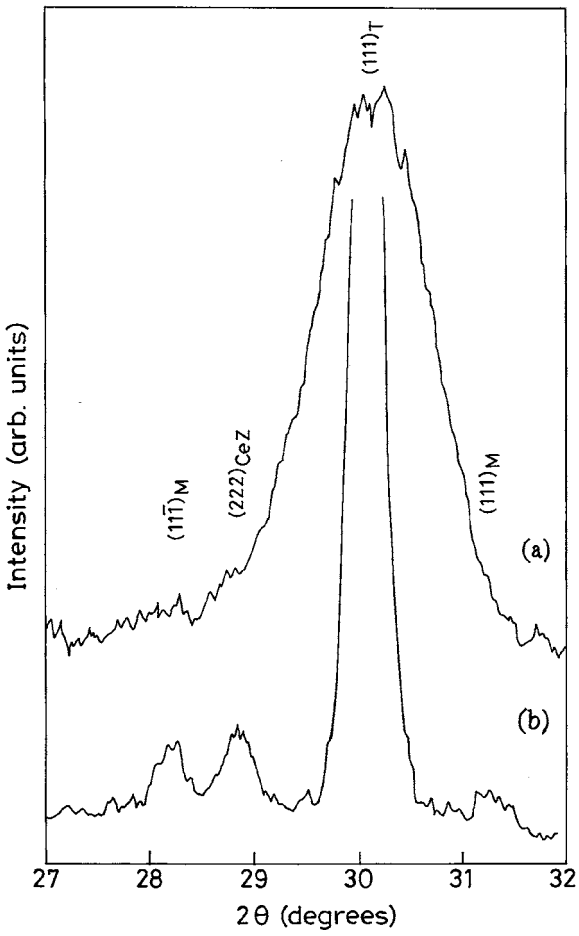

Figure 1 X-ray diffractograms of Al_2O_3-13.8 vol% ZrO_2 composites; (a) calcined powder and (b) sintered specimens (T = Tetragonal, M = Monoclinic and CeZ = $Ce_2Zr_2O_7$).

diameter 25 mm and height 4 to 4.5 mm at a pressure of 250 MPa. The pellets are held at 620°C for 1 h to remove binder and subsequently sintered at 1600°C for 1 h in air.

3. Characterization

The sintered density of the specimens is measured by Archimedes method using water as immersion liquid. The different phases present in the calcined powder as well as in the sintered specimen are identified by X-ray diffraction (XRD) using a X-ray diffractometer (Isodebyeflex 2002, Reich Seifert, Germany) with Ni filtered Cu K_α radiation.

The calcined composite powder is found to contain, besides ZrO_2, a small amount of $Ce_2Zr_2O_7$ (Fig. 1a). In the present investigation, $Ce(NO_3)_3 \cdot 6H_2O$ is used as the precursor for CeO_2 where Ce is present in +3 valence state. Calcination in air is unable to convert Ce^{3+} to Ce^{4+} completely, leaving behind some Ce^{3+} which is thought to be responsible for the formation of $Ce_2Zr_2O_7$. The zirconate phase persists in the sintered specimens (Fig. 1b). The amount of $Ce_2Zr_2O_7$ varies from specimen to specimen depending on the position in the sintered disk from where the specimen is cut. Its amount is found to be more in the bars cut from the interior of the sintered disk due to lower availability of O_2 during sintering. An estimate of the relative amount of the zirconate phase, X_{Zt}, can be made using the relation

$$X_{Zt} = \frac{I_{Zt}}{I_{Zr}} \tag{1}$$

where,

$$I_{Zr} = I_{m(11\bar{1})} + I_{m(111)} + I_{t(111)} \tag{2}$$

Here, I_{Zt} is the intensity of $Ce_2Zr_2O_7$ peak corresponding to (222) line and $I_{m(hkl)}$ and $I_{t(hkl)}$ are the peak intensities of monoclinic and tetragonal ZrO_2 corresponding to (*hkl*) line respectively. To identify the effect of cerium zirconate on the mechanical properties and microstructure of Al_2O_3-ZrO_2 composites the specimens are classified into two groups for each ZrO_2 content in the composites.

Set I: Specimens having low zirconate ($X_{Zt} < 0.05$)

Set II: Specimens having high zirconate ($0.1 < X_{Zt} < 0.2$)

The actual amount of zirconate present in the different set of specimens characterized here is given in Table I.

ZrO_2 exists in all the specimens in the monoclinic and tetragonal forms. The relative volume fraction of the monoclinic phase, V_m, is obtained using the relation [6, 7]

$$V_m = \frac{P \cdot X_m}{1 + (P - 1)X_m} \tag{3}$$

where,

$$X_m = \frac{I_{m(11\bar{1})} + I_{m(111)}}{I_{m(11\bar{1})} + I_{m(111)} + I_{t(111)}} \tag{4}$$

Here, $I_{m(hkl)}$ and $I_{t(hkl)}$ are the peak intensities of the monoclinic and the tetragonal ZrO_2 corresponding to (*hkl*) line respectively. The value of P is taken to be 1.311 [7].

For microstructural observation, the specimens are polished and thermally etched at 1320°C for 30 minutes. They are observed in a scanning electron microscope (Model JSM 840A, JEOL, Japan). The size of the Zr rich grains is taken to be the diameter corresponding to the circle of equivalent area. Stereological conversion for grain size distribution from 2 dimensional (2D) planar surface to representative 3D distribution is done [8]. The average size of Zr rich grains is

TABLE I Zirconate content (X_{Zt}) in different set of specimens

ZTA	Set I				Set II		
Vol% ZrO_2	8	11	13.8	16.5	8	11	13.8
X_{Zt}	0.03–.05	0.02–.03	0.02–.03	0.02–.04	0.13–.18	0.12–.19	0.18–.20

TABLE II Density (ρ) of set I and set II specimens containing different vol% zirconia

ZTA	Set I				Set II		
Vol% ZrO_2	8	11	13.8	16.5	8	11	13.8
ρ (gm/cc)	4.10–4.13	4.15–4.17	4.18–4.22	4.24–4.27	4.08–4.10	4.12–4.16	4.15–4.19

calculated from the distribution. The average grain size of Al_2O_3 is measured by mean intercept length method taking about 300 grains. A multiplying factor of 1.56 is used and correction is made for the presence of second phase [9]. Cracks produced on the polished surfaces of the composites by indenting with a Vickers indentor at a load of 30 Kg are observed.

Rectangular bars having dimensions 1.2 mm × 1.8 mm × 12–15 mm are cut from the sintered disks using a low speed saw and are polished to 1 μm finish. These are tested in three point bending with a span length of 7 mm for determining the fracture strength (σ_f). Fracture toughness (K_{IC}) is measured by the single edge notch beam (SENB) technique in three point bending on polished specimens having dimension 1 mm × 3 mm × 12–15 mm. The notch depth is half of the specimen depth.

4. Results

4.1. Density

The sintered densities of the composites containing different vol% ZrO_2 are given in Table II. No significant effect of $Ce_2Zr_2O_7$ on densification of ZTA is observed. Little variation in density is probably due to difference in m-ZrO_2 and $Ce_2Zr_2O_7$ contents in the two sets of specimens.

4.2. Phases and transformability

The transformability i.e. the extent of t → m transformation of t-ZrO_2 during fracture together with pre-existing monoclinic phase present in the composite is shown in Fig. 2. The amount of monoclinic phase present in the composites does not vary much with vol% ZrO_2 in set I specimens whereas it increases from ~11 to ~19% when ZrO_2 content increases from 8 to 13.8 vol% in set II specimens. Composites containing lower amount of zirconate (set I) show more transformability for intermediate ZrO_2 content. However, in set II specimens no significant change in transformability with vol% ZrO_2 is observed. Moreover, the transformability is lower than that observed in set I specimens.

4.3. Fracture toughness (K_{IC})

The plots of fracture toughness with vol% ZrO_2 for two sets of specimens are shown in Fig. 3. In case of set I specimens, a peak in K_{IC} is observed at intermediate values of ZrO_2 content. For set II composites, the K_{IC} is consistently higher and increases continuously with ZrO_2 content upto 13.8 vol% ZrO_2. A maximum K_{IC} of 8.5 MPa$\sqrt{m}$ is observed in set II as compared to 6.8 MPa$\sqrt{m}$ in set I specimen at 13.8 and 11 vol% ZrO_2, respectively.

4.4. Fracture strength (σ_f)

The plots of strength with vol% ZrO_2 are shown in Fig. 4. In set I composites, the fracture strength drops from ~500 MPa to 380 MPa when vol% ZrO_2 increases from 8 to 11 vol% and then increases to 540 MPa at 16.5 vol% ZrO_2. The dip in strength at 11 vol% ZrO_2 coincides with increase in K_{IC} in set I specimens. For

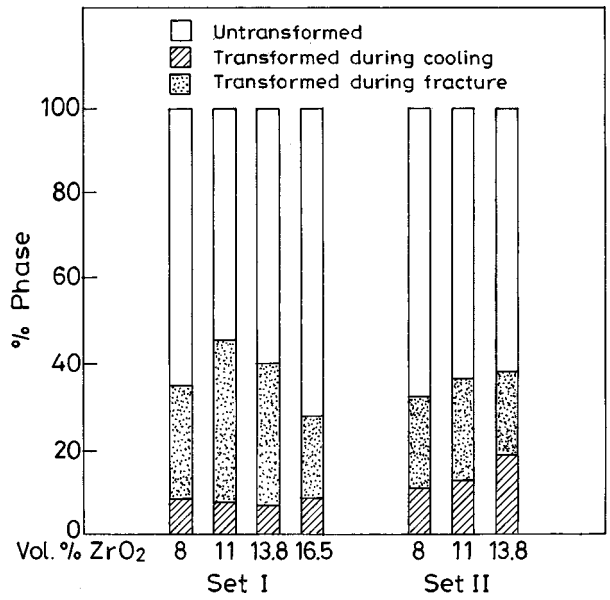

Figure 2 Bar chart showing the relative amounts of t-ZrO_2 (i.e. untransformed, transformed to m-ZrO_2 during cooling from sintering temperature and transformed to m-ZrO_2 during fracture) in different set of specimens.

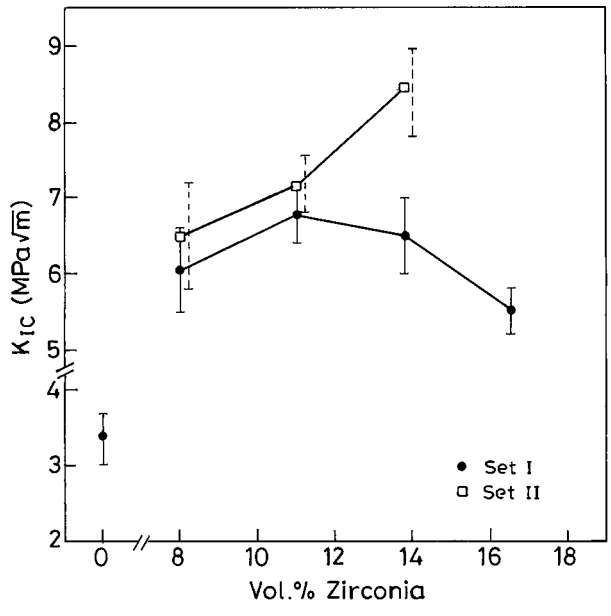

Figure 3 Fracture toughness (K_{IC}) vs vol% ZrO_2. Data points of set II specimens have been shown by broken lines and shifted slightly to the right for clarity.

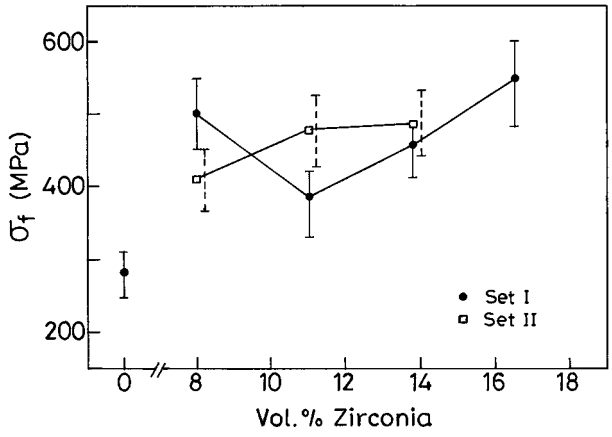

Figure 4 Fracture strength (σ_f) vs vol% ZrO_2. Data points of set II specimens have been shown by broken lines and shifted slightly to the right for clarity.

set II composites, the fracture strength increases from 410 MPa at 8 vol% to 475 MPa at 11 vol% ZrO_2 and a little change is observed with further increase in ZrO_2 to 13.8 vol.

4.5. Microstructure

The microstructures of the polished surfaces of composites containing 13.8 vol% ZrO_2, belonging to set I and set II are shown in Fig. 5. The Zr rich regions have a bright contrast. It is seen that, in the composites with low zirconate content (set I) equiaxed Zr rich grains are uniformly distributed and are located intergranularly. In the set II specimens, the Zr rich grains are well dispersed but the shape, size and morphology are remarkably different than in set I. Zr rich grains located at the Al_2O_3 grain junctions are found to be much larger as compared to such grains observed in set I. Moreover, fine and spherical Zr rich grains are observed to be present within Al_2O_3 grains. Although the location of zirconate has not been identified, however, its influence on microstructure is found to be dramatic in the composite. The Al_2O_3 grains of uniform shape are distributed within a narrow size range in set I specimens. On the contrary, considerable grain growth of Al_2O_3 is seen to occur in set II specimens. Similar microstructures are observed in two set of specimens at other vol% ZrO_2 also. The average size of Zr rich and Al_2O_3 grains in

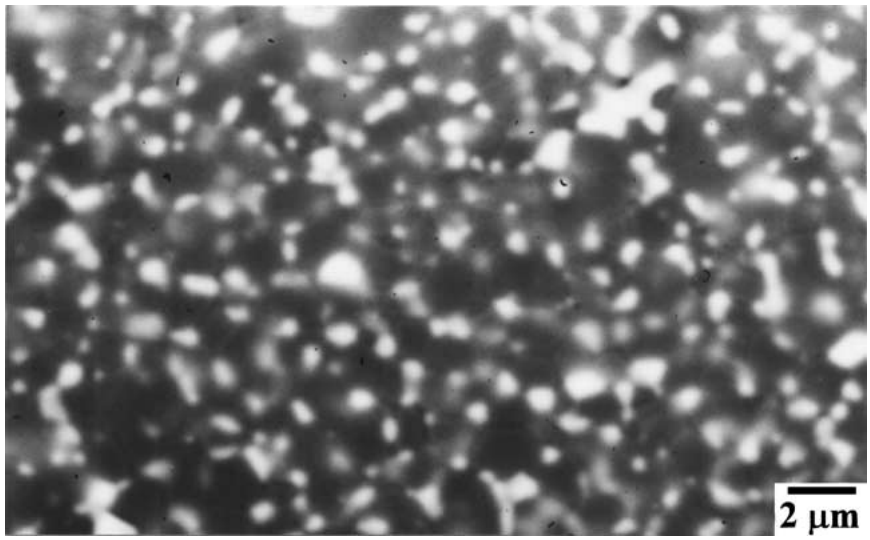

(a)

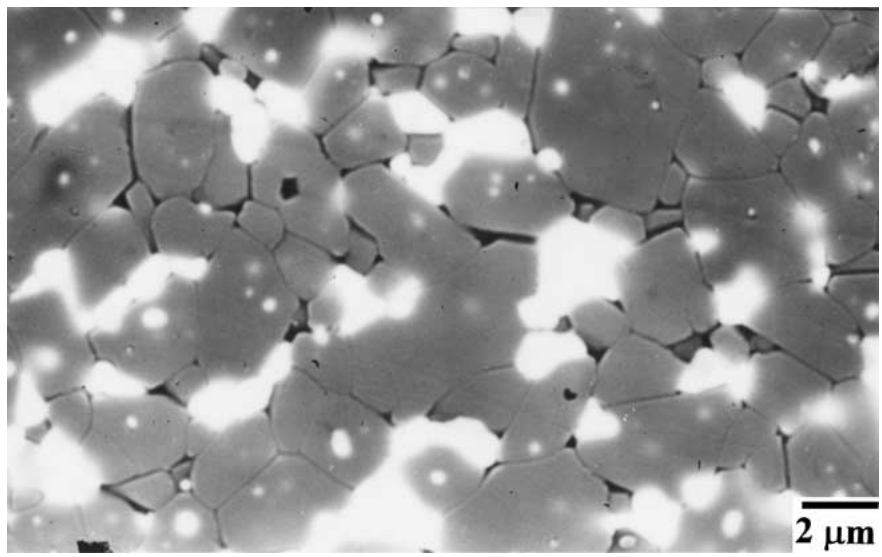

(b)

Figure 5 Microstructure of Al_2O_3-13.8 vol% ZrO_2 composites containing (a) low (Set I) and (b) high (Set II) zirconate content.

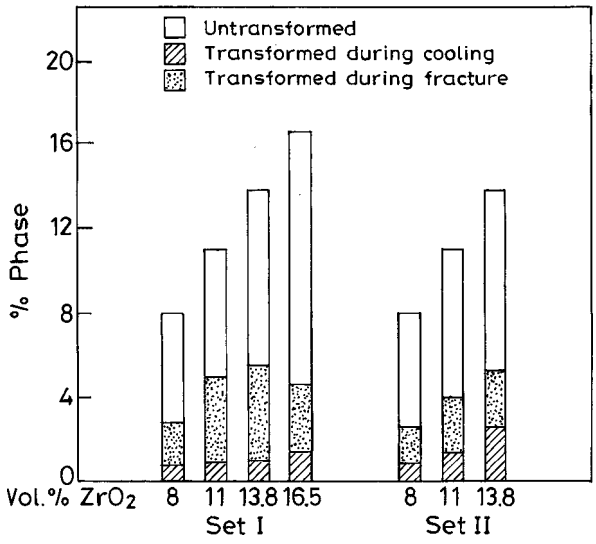

Figure 6 Bar chart showing the amounts of t-ZrO_2 (i.e. untransformed, transformed to m-ZrO_2 during cooling from sintering temperature and transformed to m-ZrO_2 during fracture) in different set of specimens.

TABLE III Grain sizes of Al_2O_3 ($d_{Al_2O_3}$) and Zr rich phases (d_{ZrO_2}) in different set of specimens

	Set I			Set II		
Volume% ZrO_2	$\bar{d}_{Al_2O_3}$ (μm)	d_{ZrO_2} (μm)		$\bar{d}_{Al_2O_3}$ (μm)	d_{ZrO_2} (μm)	
		$\bar{d}_{ZrO_2}$	σ_{ZrO_2}		$\bar{d}_{ZrO_2}$	σ_{ZrO_2}
8	2.0	0.40	0.13	3.5	0.60	0.27
11	1.6	0.50	0.15	3.1	0.60	0.31
13.8	1.4	0.55	0.15	2.7	0.65	0.39
16.5	1.3	0.55	0.17			

two sets of specimens with different vol% ZrO_2 are given in Table III.

5. Discussion

The mechanical properties of ZTA largely depend on the phases of ZrO_2 present as this ultimately determines the toughening mechanism operative in the

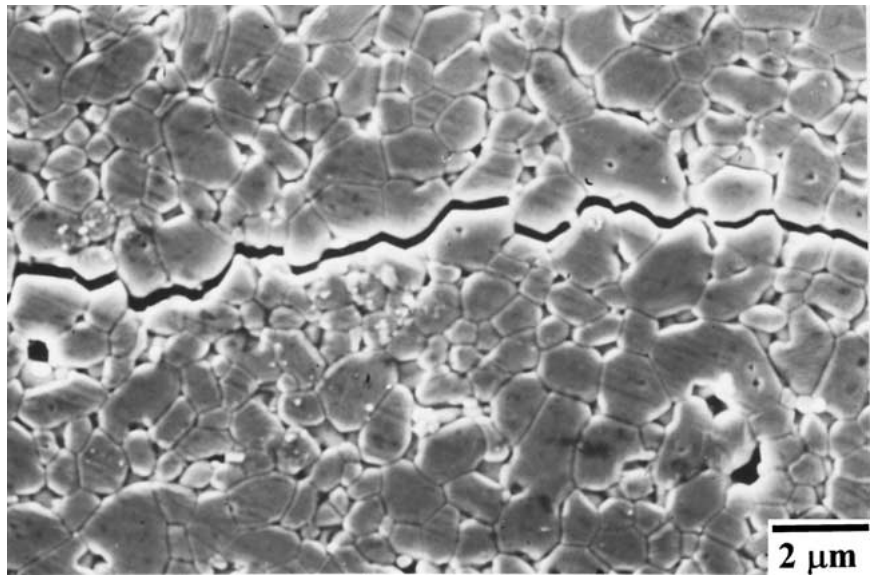

(a)

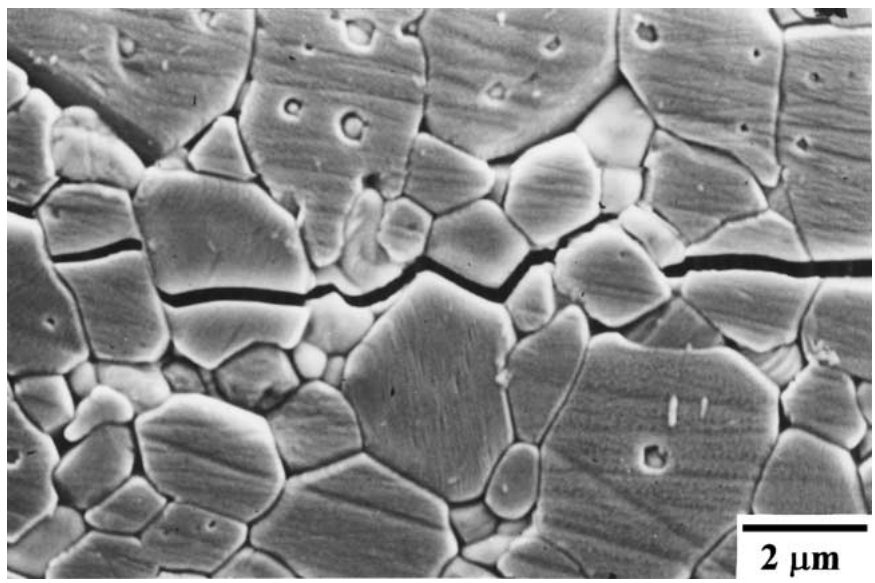

(b)

Figure 7 Indentation crack in Al_2O_3-13.8 vol% ZrO_2 composite; (a) in set I specimen at 110 μm from the crack tip and (b) in set II specimen at 120 μm from the crack tip.

composite. The presence of microcracks is known to improve the fracture toughness and degrade the strength [10, 11], whereas the stress induced t → m transformation enhances both K_{IC} and σ_f in the composite [12–15], although the peak values of K_{IC} and σ_f may occur at different ZrO_2 contents [13–15]. In our specimens, besides tetragonal and monoclinic ZrO_2, an additional phase i.e. $Ce_2Zr_2O_7$ is observed to form. The fracture toughness behaviour of set I specimens, in general, follows the absolute amount of t-ZrO_2 transformed during crack propagation (Fig. 6). Higher values of K_{IC} are observed at 11 and 13.8 vol% ZrO_2 where the transformation of the tetragonal phase is also higher. However, the σ_f of the set I specimens is seen to be lower where higher values of toughness are achieved and vice versa. The reasons for this are not understood at present.

On the other hand, specimens with higher zirconate contents (set II) display the presence of higher amount of pre-existing m-ZrO_2 and lower transformability during fracture. The formation of $Ce_2Zr_2O_7$ phase lowers the CeO_2 content available for the stabilization of t-ZrO_2 thereby resulting in the formation of higher amount of m-ZrO_2 in the as sintered composites. Lower transformability of t-ZrO_2 during fracture due to presence of zirconate (Nd-zirconate, La-zirconate) is also reported in Ce-TZP [16]. Microstructures of the set II specimens reveal large grain growth of Al_2O_3 with fine Zr rich particles within Al_2O_3 grains. Increased mobility of Al_2O_3 grain boundaries due to the presence of Ce^{3+} in ZrO_2 has been reported [4]. A similar effect seems to be present here due to the presence of Ce^{3+} in zirconate.

The most significant observation in set II specimens is that, they exhibit higher toughness despite lower transformability of t-ZrO_2 compared to that in set I specimens (Figs 3 and 6). Although higher amount of m-ZrO_2 (compared to set I) is formed but the contribution of microcracking as a result of pre-existing monoclinic phase may not be high enough to account for better toughness in set II specimens. Moreover, it should lead to a degradation in strength which is not observed. Thus it appears that the presence of zirconate phase promotes some toughening mechanisms other than transformation toughening and microcracking.

Enhancement in toughness of Al_2O_3 ceramics due to crack bridging has been reported by several investigators [17–20]. In the set II specimens also, it seems that the significant contribution to fracture toughness is from crack bridging. Fig. 7 shows the images of the cracks produced by a Vickers indentor. No bridging site is seen in the composite containing low zirconate (Fig. 7a) while in high zirconate specimens, crack bridging sites with transgranular fracture of Al_2O_3 grain are observed and continue to persist at a large distance from the crack tip (Fig. 7b). Thus the modification of microstructure due to presence of zirconate leads to crack bridging mechanism to be operative with other toughening mechanisms resulting in increase in toughness without any degradation in strength.

6. Conclusion

Formation of zirconate ($Ce_2Zr_2O_7$) phase is found to occur in the sintered specimens of Al_2O_3-(Ce)ZrO_2 composites. The amount of zirconate phase is maximum at the centre of the specimen where the availability of oxygen is limited by its diffusion from the surface to interior. The presence of the zirconate phase causes a growth of the Al_2O_3 grains, such that the crack bridging mechanism for toughness enhancement can operate. This helps in obtaining simultaneous high values of strenght and toughness in the composites.

Acknowledgement

Partial support for this work was provided through a grant by Department of Science and Technology, Govt. of India.

References

1. A. I. LEONOV, A. B. ANDREEVA and E. K. KELER, *Izv. Akad. Nauk. SSSR, Neorg. Mater.* **2** (1966) 137.
2. K. H. HEUSSNER and N. CLAUSSEN, *J. Amer. Ceram. Soc.* **72** (1989) 1044.
3. H. Y. ZHU, T. HIRATA and Y. MURAMATSU, *ibid.* **75** (1992) 2843.
4. L. A. XUE, K. MEYER and I. W. CHEN, *ibid.* **75** (1992) 822.
5. A. SAHA, D. C. AGRAWAL and A. SHARMA, in "Ceramic Transactions" Vol. 38, edited by N. P. Bansal (American Ceramic Society, Westervillie, OH, 1994) p. 497.
6. H. K. SCHMID, *J. Amer. Ceram. Soc.* **70** (1987) 367.
7. P. A. EVANS, R. STEVENS and J. G. P. BINNER, *Trans. J. Brit. Ceram. Soc.* **83** (1984) 39.
8. R. T. DEHOFF, "Fifty Years of Progress In Metallographic Technique," ASTM STP no 430 (American Society for Testing and Materials, Philadelphia, Pennsylvania, 1968) p. 63.
9. J. C. WURST and J. A. NELSON, *J. Amer. Ceram. Soc.* **55** (1972) 109.
10. N. CLAUSSEN, *ibid.* **59** (1976) 59.
11. *Idem., ibid.* **61** (1978) 85.
12. Y. MATSUMOTO, K. HIROTA, O. YAMAGUCHI, S. INAMURA, H. MIYAMOTO, N. SHIOKAWA and K. TSUJI, *ibid.* **76** (1993) 2677.
13. S. HORI, M. YOSHIMURA, S. SOMIYA, R. KURITA and H. KAJI, *J. Mater. Sci. Lett.* **4** (1985) 413.
14. H. YOSHIMATSU, Y. MIURA, A. OSAKA, H. KAWASAKI and O. OHMORI, *J. Mater. Sci.* **25** (1990) 5231.
15. M. V. SWAIN and L. R. F. ROSE, *J. Amer. Ceram. Soc.* **69** (1986) 511.
16. K. TSUKUMA, *Am. Ceram. Soc. Bull.* **65** (1986) 1386.
17. P. L. SWANSON, C. J. FAIRBANKS, B. R. LAWN, Y. W. MAI and B. J. HOCKEY, *J. Amer. Ceram. Soc.* **70** (1987) 279.
18. N. P. PADTURE, J. L. RUNYAN, S. J. BENNISON, L. M. BRAUN and B. R. LAWN, *ibid.* **76** (1993) 2241.
19. J. HOMNEY, W. L. VAUGHN and M. K. FERBER, *Am. Ceram. Soc. Bull.* **67** (1987) 333.
20. G. C. WEI and P. F. BECHER, *ibid.* **64** (1985) 298.

Received 22 May 2000
and accepted 3 August 2001